Construction of the Photon Tagger Microscope for the GlueX Experiment

Liana Hotte

University of Connecticut – Storrs CT 06269

Honors Undergraduate Thesis, Dec 2015

Abstract

The GlueX experiment at Jefferson Laboratory (JLab) in Newport News, VA is conducting a search for a new type of particle called an exotic meson. Exotic mesons are predicted to exist by the Standard Model of Particle Physics. Experiments searching for exotic mesons have reported evidence for their existence over the past 25 years, and recently the LHC at CERN has produced the first definitive confirmation of their existence. GlueX is designed to produce them in large numbers so that their mass spectra can be determined and other properties studied. To do this, GlueX requires a beam of high-energy polarized photons which are generated by passing high-energy electrons from the JLab accelerator through a thin diamond crystal. The photon energies are then "tagged" by measuring how much energy the electrons lost in the crystal. This function is provided by the tagger microscope, a highly-segmented scintillation detector which detects the degraded electrons and measures their energy and time. As electrons strike a scintillating fiber, an optical signal is transmitted to a silicon photomultiplier which converts it to an electrical signal to be digitized and recorded. The University of Connecticut successfully completed the construction and testing of the tagger microscope in 2014 and delivered it to JLab, where it is now operating as part of the GlueX experiment in its first year running.

Table of Contents

Table of Figures

1. Introduction

The primary scientific goal of the GlueX experiment is to map the mass spectra of particles produced from photon/hydrogen interactions in hopes of studying the properties of exotic mesons. In order to fully understand the goals of the GlueX experiment, it is helpful to review the physics discoveries which led to modern atomic and particle physics. This introduction provides a brief historical basis with the goal of better understanding the importance of the GlueX experiment.

1.1. Atomic Theory

In the 1800s, the elementary component of matter was considered to be the atom. It was not until 1897 that British physicist Joseph John "J.J." Thompson, due to his work with cathode ray tubes in Cavendish Laboratory, hypothesized and confirmed the existence of the electron. He proposed that these negatively-charged subatomic particles existed in a sea of positive charge. This atomic model is famously called the plum-pudding model because it was imagined to be similar to how plums may be uniformly distributed and suspended in a plum-pudding.

In 1917, the plum-pudding atomic model was overturned by the discovery of the proton. The proton's discovery is often attributed to Ernest Rutherford and his associates at Cavendish Laboratory. Rutherford's group discovered that a beam of alpha particles aimed at a thin foil of gold atoms caused occasional backward deflections of the beam which implied there was a compact, massive center of the atom, called the nucleus. Experiments showed that the nucleus always held an integer multiple of an elementary charge, but not for atomic mass. He concluded that the nucleus consisted of subatomic particles of quantized positive charge, surrounded by empty space and electrons orbiting the nucleus. This atomic model was supported by the discovery of the neutral subatomic particle, the neutron, in 1932 by James Chadwick, which explained how the nucleus' positive charge was quantized while the atomic mass did not follow the same quantization. This atomic model which consisted of a nucleus and orbiting electrons is called the Rutherford Model (or the planetary model due to its similarity to a planet with orbiting moons).

The formulation of quantum mechanics was not until the 1920s, at which point the atomic model was again renovated. Erwin Schrodinger published his paper including his namesake equation in 1926 which described how electrons do not move in discrete orbitals, as previously hypothesized, but rather exist in a wave-function which describes the probability of finding the electron at a specific location. With the acceptance of quantum mechanics came the modification of the atomic theory from discrete electron orbitals to electron clouds, which reigns as the atomic model today.

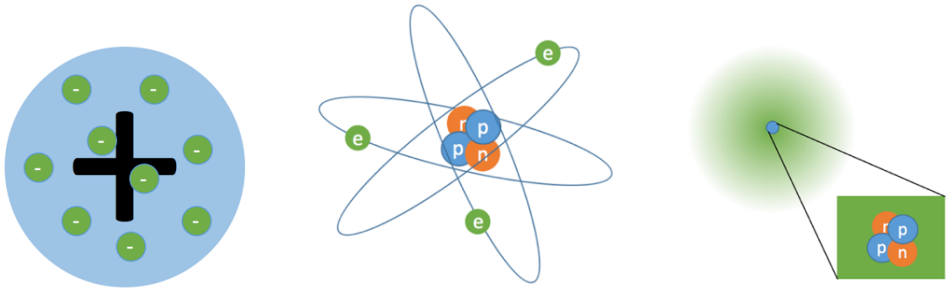

FIGURE 1. Left: The *plum-pudding model*, where small negative charges float in a sea of positive charge. Center: The *Rutherford model*, a compact nucleus consisting of protons and neutrons surrounded by electrons in discrete orbits. Right: The modern *quantum model*; a nucleus composed of protons and neutrons surrounded by a probability cloud to describe electron motion.

1.2. Particle Physics

In the years following the discoveries of first subatomic particles, scientists found more particles and studied their properties in great depth. However, it was not until 1964 that Gell-Mann, Zweig, and Okubo first proposed the quark model, which described how these particles (proton, neutron, pion, kaon…) are composed of point-like structures and how those structures interact with the fundamental forces of nature. The quark model was confirmed shortly after, in the late 1960s/early 1970s, when a team at the Stanford Linear Accelerator Center (SLAC) performed a series of deep inelastic scattering experiments which probed protons and proved they had internal structure. Since then, many experiments have contributed to the confirmation and expansion of the fundamental particles model, which resulted in the Standard Model of Particle Physics. The Standard Model is the leading theory which describes the smallest units of matter and their interactions with the strong, weak, and electromagnetic forces. It includes twelve fermions (six quarks and six leptons) which compose all matter, four force-carrying gauge bosons, and the Higgs boson. These fermions and bosons are all organized in a table analogous to the periodic table, by mass and generation in Figure 2.

Quantum chromodynamics (QCD) is the theory of interactions between quarks/anti-quarks and the strong force carriers, gluons. Analogous to how electrically charged particles interact through electromagnetic forces, quarks have a property called color charge which allow them to interact through the strong force (which explains the *chromo* in QCD). One may assume that color charge is perhaps the same as optical color, but this is not true; color charge is just an easy nomenclature for the effects observed. Quarks may have one of three color varieties: red, green or blue. And similar to optical color, the combination of a red, green, and blue quark is said to be white or color neutral. Just as quarks have color, anti-quarks hold anti-color. Gluons also carry both color and anti-color, meaning they can interact with quarks, anti-quarks, and themselves.

One concept QCD is supposed to explain is color confinement, which is the phenomenon of hadrons only existing in color-neutral configurations. Simple baryons and anti-baryons consist of 3 quarks or anti-quarks and achieve color neutrality by having a {red, green, blue} or {anti-red, anti-green, anti-blue} color configuration. Simple mesons consist of a quark-antiquark pair with a color neutral {color/anti-color} configuration.

Color confinement has yet to be proven analytically, but it is speculated to be true because of the empirical fact that no one has ever observed an isolated, free quark. QCD is asymptotically free, meaning the strong force becomes asymptotically weak at large energies and small distances. Conversely, when the quarks in a color-neutral configuration are separated by an increasing distance, gluons between them create a tube/string of chomo-magnetic flux between the two quarks. Eventually, the energy to elongate the gluon tube becomes greater than the energy to create a quark/anti-quark pair. This means that if you inject enough energy into a quark-antiquark pair, the result will be *two* quark-antiquark pairs.

The gluonic field which holds quarks and antiquarks together can be excited according to the flux-tube model. The GlueX experiment hopes to find exotic hybrid mesons, or mesons with vibrating gluonic flux tubes and also glueballs, isolated excitations of the gluonic field. These types of states are going to be studied by mapping the spectra of mesons.

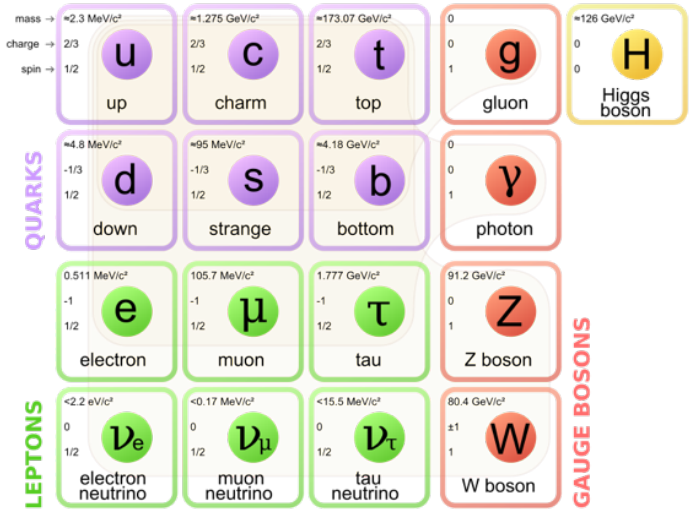

FIGURE 2. The quarks, leptons, and bosons of the Standard Model.
Each has a mass, charge, and spin. Image courtesy of Wikipedia article “The Standard Model”.

2. GlueX

Jefferson Lab is the U.S. Department of Energy national laboratory which houses the Continuous Electron Beam Accelerator Facility (CEBAF), which produces a high-energy electron beam. In 2014, upgrades to CEBAF were completed to increase the electron beam energy to 12 GeV and add Hall D, where GlueX is housed (See Figure 3).

GlueX is a particle physics experiment whose purpose is to map the spectrum of hybrid mesons, including those with exotic and unique quantum numbers. Hybrid mesons will be created through a process called photoproduction, which involves bombarding hadrons with high-energy photons. The high-energy photon beam is created by bremsstrahlung radiation, a process which produces photons from the deceleration of electrons.

CEBAF's 12 GeV electron beam enters Hall D and passes through a 20-micron thin diamond wafer. As the high-energy electrons scatter from carbon atoms in the diamond crystal, they release some of their energy in the form of bremsstrahlung radiation. The photon beam continues down the hall to a liquid hydrogen target and subsequent detectors in hopes to detect the shower of mesons produced, while the final lower-energy electron beam is deflected in the photon tagging spectrometer.

It is essential to know the energies of the photons in order to know that one has correctly accounted for all of the particles produced in the reaction, but their energies cannot be measured directly without destroying the photons. In order to indirectly measure the photon energies, the photon tagger measures the energies of the slowed electrons and photon energies are inferred based on energy conservation.

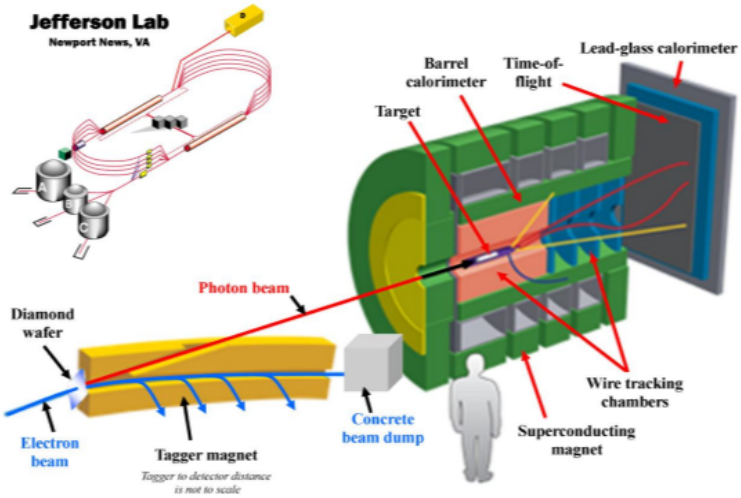

FIGURE 3. Upper-left: An overview of JLab's accelerator including the recently added Hall D. Lower: A diagram showing the path of the beams.

2.1. Description of Photon Tagger Microscope

In order to separate the bremsstrahlung electrons from the photons, a magnetic field is applied by the tagger magnet to deflect the electron beam to the tagger microscope detector. This deflection is possible because of the Lorentz force due to a magnetic field (Eq. 1).

$$\vec{F} = q\vec{v}\times\vec{B} \tag{1}$$

As photons hold no electric charge (***q***=0), they experience zero Lorentz force and pass through the magnetic field un-deflected. However, the electrons have both charge and velocity, so they undergo a deflection due to the magnetic field. This deflection of the electrons separates the photons continuing to the liquid hydrogen target from the electrons curving towards the photon tagger microscope.

The Lorentz force equation (Eq. 1) shows that the deflection of the electrons depends on their charge and momentum. Electrons with different velocities will experience different magnitudes of the Lorentz force. The tagger measures the electron momentum in the following way.

Due to the electrons' high energies, they travel at nearly the speed of light. As a result, relativistic effects must be accounted for. The relativistic energy expression is in the form of Eq. 2 but is simplified to Eq. 3 when particles have large enough momenta ***p*** to make the rest mass $\boldsymbol{m_o}$ become negligible.

$$E = \sqrt{|\vec{p}|^2c^2 + {m_o}^2c^4} \tag{2}$$

$$E \approx |\vec{p}|c \tag{3}$$

Now consider the relativistic momenta expression (Eq. 4).

$$|\vec{p}| = \frac{m\vec{v}}{\sqrt{1-\frac{|\vec{v}|^2}{c^2}}} \tag{4}$$

The relationship between velocity and momenta in Eq. 4 states that small changes in velocity result in large changes in momentum. As stated in Eq. 3, a large change in momentum would create a large change in energy. This means that despite the range of electron energies, the velocities of the bremsstrahlung electrons are essentially the same.

So if the bremsstrahlung electrons all have the same charge, and essentially the same velocities, they will all experiencing the same Lorentz force. So how does the photon tagger separate the electrons by energy? Although the electrons will experience the same Lorentz force, they will not all deflect through the same angle. Recall that force is the time-derivative of momentum and apply it to Eq. 1.

$$\frac{d\vec{p}}{dt} = q\vec{v}\times\vec{B} \tag{5}$$

$$d\vec{p} = \left(q\vec{v}\times\vec{B}\right)dt \tag{6}$$

Equation 6 shows that the instantaneous change in momentum ***dp*** is the same for all electrons because ***q***,***v***,***B***,***dt*** are the same for all electrons (***dt*** is the same because of the similar velocities). It is also true that the change in momentum will be perpendicular to the velocity because of the cross product in Eq. 6. This means that the deflection angle of the bremsstrahlung electrons depends on the initial momentum of the electrons. This conclusion is easily understood by looking at Figure 4.

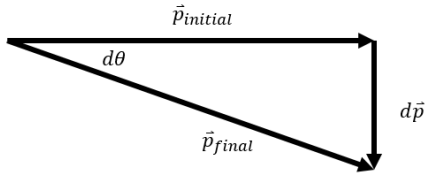

FIGURE 4. A diagram showing how the deflection angle of the bremsstrahlung electrons depends on the initial momenta.

The deflected angle, ***dθ*** is calculated using the arctangent function as in Equation 7.

$$d\theta = \tan^{-1}\left[\frac{|d\vec{p}|}{|\vec{p}_{inital}|}\right] \tag{7}$$

In conclusion, the electrons' deflection angles depend on their initial momenta and their initial momenta depend on their energies so the tagger microscope can detect differences in electron energies by detecting the differences in their deflection angles.

Because the photon tagger microscope must have a high resolution in detecting electron energies (at least 0.1% energy resolution) with low pulse overlap, the microscope must be designed in such a manner that it can detect very small spatial differences in the electron deflection. In order to achieve such high resolution, the photon tagger microscope consists of 510 scintillating fibers, each with a cross sectional area of 2mm x 2mm. In order to optimize light yield and minimize cross-talk, the scintillating fibers were cut to 2cm long and fused to a clear waveguide which transmits the signal to the photo-sensors. The fibers were arranged in an array 102 fibers long x 5 fibers high. This array allows the microscope to detect electrons with small vertical displacement, and detect electrons in the range from 3.0-3.6 GeV.

The bremsstrahlung electrons are detected when they interact with the dopants of the scintillating fibers. The dopant molecules of the fibers become excited due to the collision and scintillate when relaxing back to the ground state. The scintillation produced travel through the fused light guide

(which does not detect electrons but only carries the light signal) out of the incoming plane of electrons. The light is directed to the silicon photomultiplier (SiPM) detectors where they are converted to an electric pulse and recorded for analysis.

3. Fiber Production

3.1. Optical Fiber Properties

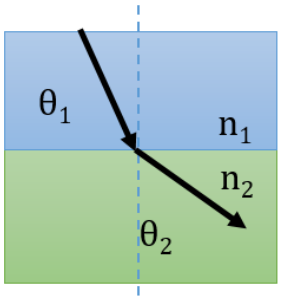

FIGURE 5. A ray of light passing from medium with index of refraction n_1 to a medium with index of refraction n_2 where $n_2 < n_1$.

The speed of light, the maximum speed that light travels in a vacuum, is defined to be 299,792,458 m/s. When light interacts with matter, it propagates at a slower velocity due to collisions with molecules. The property of matter which describes the retardation of light propagation is called the index of refraction, generally denoted as ***n***. The index of refraction of a material is calculated by dividing the speed of light in a vacuum by the speed of light in a material, as in Eq. 8.

$$n = \frac{c}{v} \tag{8}$$

When light enters a new medium, the light rays are deflected or "refracted". The relation between the angle of refraction and the index of refraction of the medium is expressed in Snell's Law, Eq. 9. Figure 5 is a geometric diagram showing refraction at a medium boundary.

$$n_1 sin\,\theta_1 = n_2 sin\,\theta_2 \tag{9}$$

Snell's law shows that when a ray with angle of incidence $\boldsymbol{\theta_1}$ hits a media boundary where $\boldsymbol{n_1} > \boldsymbol{n_2}$, the ray refracts along the surface of the boundary. This angle is called the critical angle $\boldsymbol{\theta_c}$, and can be found using Eq. 10.

$$\theta_c = sin^{-1}\left(\frac{n_2}{n_1}\right) \tag{10}$$

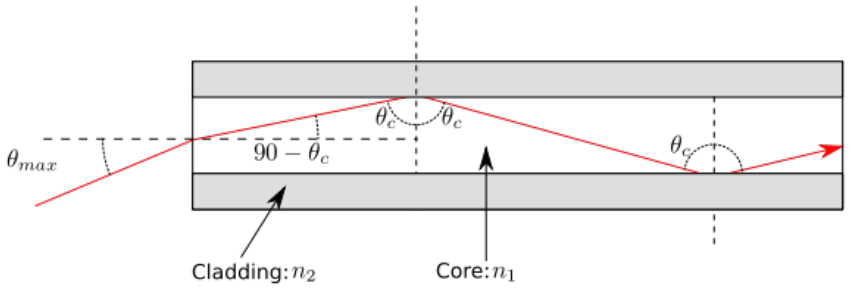

FIGURE 6. Light ray diagram of light entering a single-clad optical fiber and being repeatedly internally reflected off the cladding layer.

When the angle of incidence surpasses the critical angle, a phenomenon called total internal reflection occurs. When $\boldsymbol{\theta_1} > \boldsymbol{\theta_c}$, the light ray is totally reflected off the media boundary. Optical fibers rely on this effect to contain and relay light signals. Figure 6 is a diagram which shows the geometry of a light ray travelling within an optical fiber with a single cladding layer. For the optical fibers to retain the light by total internal reflection, it is necessary that the cladding material have an index of refraction lower than the core material's index of refraction.

For the tagger microscope, Saint Gobain Ceramics & Plastics, Inc. manufactured both of the fiber types required for the project. The products used were the BCF-98 and BCF-20, the clear light guide and green scintillating fiber, shown in Figure 7. All fibers were ordered as multi-clad, meaning they had two layers of cladding around the core to ensure low attenuation. Both fibers have square profiles, measuring 2mm x 2mm. The indices of refraction for each material is listed in the table in Figure 8. The scintillating fiber core contains fluorescent dopants which result in the production of approximately 8,000 photons per MeV of a minimum ionizing particle.

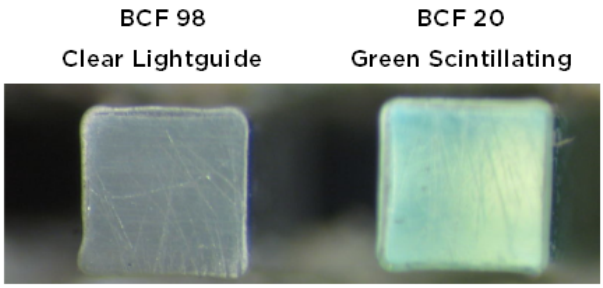

FIGURE 7. A cross-sectional view of both the clear light guides (left) and the green scintillating fibers (right).

	Material	Index of Refraction
Core	Polystyrene	1.60
First Cladding Layer	Acrylic, PMMA	1.46
Second Cladding Layer	Fluor-acrylic	1.42

FIGURE 8. A table of the materials and the indices of refraction for the Saint Gobain Inc. optical fibers, both the BCF-98 and the BCF-20.

3.2. Cutting/End milling

The Saint Gobain Inc. optical fibers were shipped on a large cardboard spool. They were stored in the UConn labs suspended off the ground for easy unraveling of the fibers without inducing strain. The first step in fiber production was the cutting step, where fibers were rough cut off the spool and then fine cut to precise lengths required for the detector. Scintillating fibers were cut to be approximately 2 cm long and the clear light guides were cut to be approximately 167 cm long.

The initial cut was made using a Dremel tool to rough cut the fibers to an approximate size from the spool. During the prototyping phase, a hot knife was used to make this cut but it was quickly determined that the fiber was too thick. The time required for the hot knife to make the cut was too long - the area around the cut melted and deformed. The rough cut provided by the Dremel provided quick and clean cuts, meaning the cladding incurred minimal damage, see Figure 9.

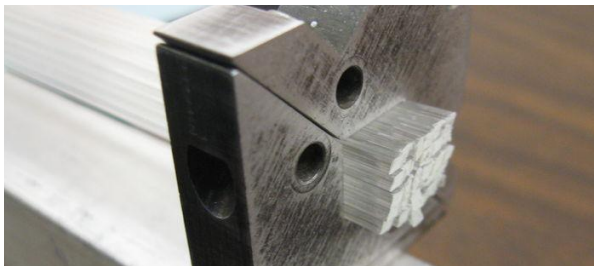

FIGURE 9. An image of a bundle of light guides after being individually rough cut with the Dremel tool. The cuts are not perpendicular, but there is little to no damage of the cladding.

After the fibers were rough cut, a finer cut was required to shorten the fibers to the specified length for the detector. The fine cut was achieved by tightly bundling the fiber ends using custom fiber collars and using an end-mill to mill the fibers down to length. A double-fluted ⅜-inch end mill at 1400 RPM was used to cut the fibers, shown in Figure 10. Approximately 0.01-0.02 cm of fiber was end-milled per pass, so multiple passes over the fibers were required. Between each pass, the fiber debris had to be cleared, otherwise the residual fiber would be ground underneath the cladding of the fibers.

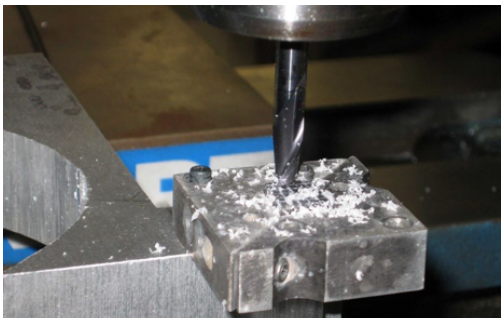

FIGURE 10. The light guides are being milled to specified length. The fiber debris must be cleared before the next pass of the end mill over the fiber end surface.

3.3. Indexing, Measurements and Storage

After fibers were cut from the spool to length, the fibers were then bundled (grouped), indexed, measured, and stored. From this point onward, fibers were processed in “bundles” or groups of 30 due to the design of the microscope. Every fiber was given a unique ID which consisted of it’s bundle number, and its fiber number.

The cross-sectional widths for every clear light guide were measured in 5 places along the fiber (about 40 cm between measurement locations) and measured in the center of every scintillating fiber. Special care was taken to ensure that each width recorded was matched to the fiber ID to track any possible changes in cross-section between processes.

The optical fiber bundles were then placed in a fabric-covered wooden storage unit, shown in Figure 11. This ensured the fibers were not being scratched by any abrasive material and were kept in a clean, dark location.

FIGURE 11. A photo of the intermediate storage box for the fibers in production.

3.4. Straightening

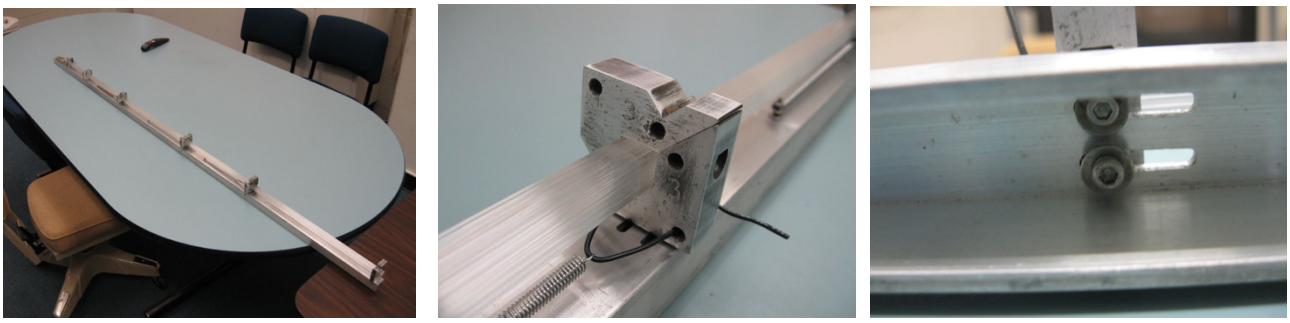

FIGURE 12. Images of the straightening equipment. Left: The aluminum straightening bar with six fiber collars. Center: A view of a spring applying tension to the fiber collar. Right: The bottom of the straightening bar revealing the slots where the fiber collars with springs have room to move with the fiber as it is straightened.

In order to fuse the scintillating fiber to the light guide, the light guides had to be straightened to lay flat on the fusing unit. From being stored and shipped on the large spool from Saint Gobain, they had developed a slight curve, which complicated handling for the fusing procedure. The light guide fibers were secured to an aluminum straightening bar where springs applied a small tension to the fibers as they were heated in water and then cooled. This process resulted in a bundle of 30 straightened light guides.

Thirty light guides were bundled together using custom fiber collars in a 5x6 array. They were secured with collars in six places along the light guides' 167 cm length. Careful attention was given to ensure that fibers did not get tangled or change position between collars, causing kinks in the fibers. The collars were then secured to a long aluminum bar, referred to as the straightening bar. The collar at one end of the fibers was tightly secured to the straightening bar, remaining stationary. The other collars were free to slide along the bar so that fibers were pulled straight.

Once the fibers were secured with the collars and springs to the straightening bar, the bar was placed into a large PVC pipe, which was filled with room temperature water using the water system drawn in Figure 13. A LabView program was used to record the temperature of the water and control the heaters and pumps as the water was heated to 160 degrees Fahrenheit, well below polystyrene's melting point. After reaching the right temperature, the fibers cooled for 12 hours back to room temperature before being removed from the water. The temperature profile for the straightening of Bundle 1 is shown in Figure 14.

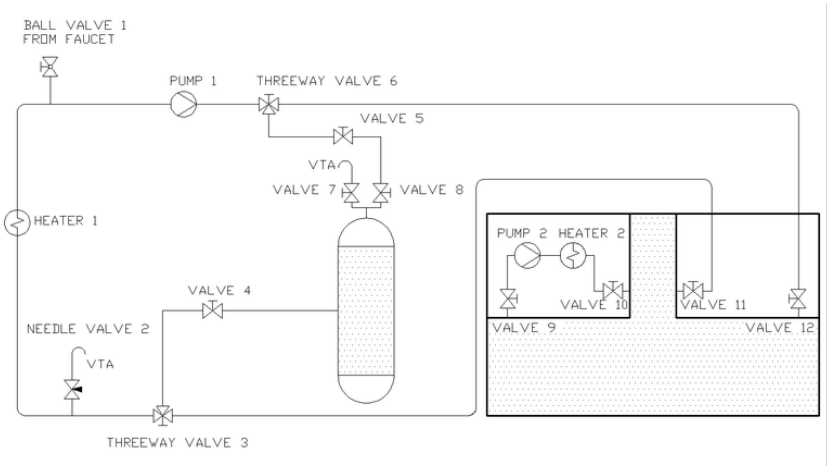

FIGURE 13. A pipe diagram of the water system used for straightening and bending fibers. It was designed to fill and heat the PVC straightening pipe and the bending tank separately.

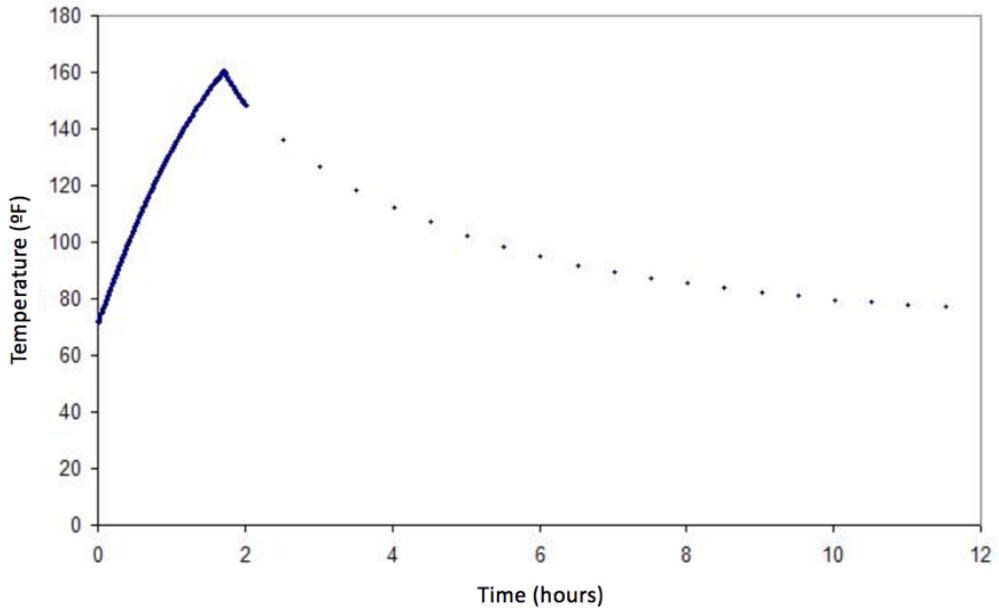

FIGURE 14. The time series throughout the straightening procedure of Bundle 1.

3.5. Cleaning and Alcohol Tests

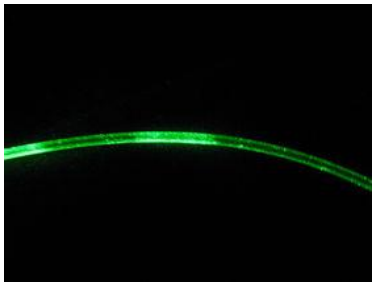

FIGURE 15. Light escaping from an optical fiber touched with bare hands.

All fiber handling was conducted while wearing gloves to prevent contaminating the fibers with biological oils whose effects as shown in Figure 15. Fibers were stored in clean, dark containers to prevent dust and damage from ambient ultraviolet light. However, it was soon determined that a cleaning procedure was required. As fibers were brought in contact with the aluminum fiber collars during straightening and milling, fibers showed signs of stress and surface degradation, most prominent of which was the rust deposits and hard water stains on the cladding of the fibers, seen in Figure 16.

In hopes of reducing these rust deposits, a water filter was added to the water input system. In addition, a cleaning procedure was incorporated into the fiber production processes. After the removal of the fibers from water (post-straightening and post-bending), the fibers were wiped with a clean lint-free cloth and a dilute alcohol mixture. This removed the hard water stains and rust deposits without causing any visible damage to the fiber cladding.

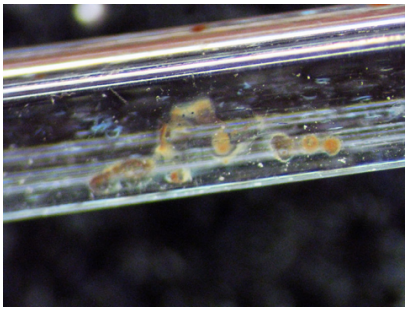

FIGURE 16. Rust spots on a light guide after straightening.

Some preliminary alcohol cleaning tests resulted in adverse effects on the fibers. Fibers were found to be free from stains, but seemed to show signs of internal stress and the fiber cladding appeared to be damaged as well. These preliminary results led to further testing of the fibers in various alcohol solutions to better understand the reaction.

Small pieces of fibers were set in solutions of 0-100% ethanol concentrations to determine the best solution for fiber cleaning. The primary methods of checking for fiber damage were visual inspection and checking for changes in fiber cross sectional widths. Oftentimes, we found fibers swelled from absorbing water or decreased in size from cladding damage. We continued these tests to include heated alcohol tests, where fibers were set in 150-180°F ethanol to mimic if any ethanol remained on the fibers during the heating process. Results showed that extreme fiber damage occurred when fibers were left in high concentration (greater than 50%) ethanol solutions, Figure 17.

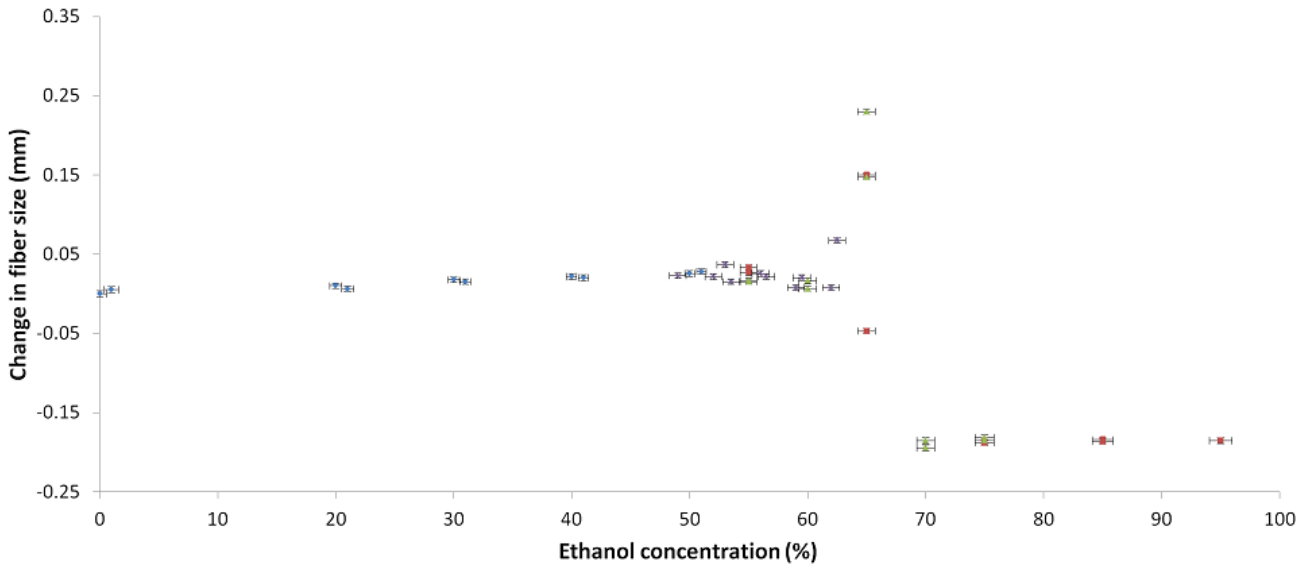

FIGURE 17. Data from a number of heated alcohol tests on fibers. The fibers were in the heated alcohol for hours to simulate the timescale of the straightening/bending processes.

An enormous change in fiber appearance occurred when fibers were placed in high concentration ethanol solutions and heated for hours. Figure 18 shows the drastic changes in the fibers after enduring these extreme tests. As a result of these heated alcohol tests, it was decided to not clean the fibers with any sort of ethanol solution but rather just use a dry, lint-free cloth.

FIGURE 18. Fibers after sitting in 75%, 65%, 55% (left to right) heated ethanol. Diameter measurements (see Fig. 17) showed that the right-most fiber shown in the photo has completely lost its cladding layer.

3.6. Polishing

As a result of the end milling process, fiber ends were perpendicularly cut and relatively smooth to the touch. However, to maximize light transmission, the fiber ends were polished to a mirror finish. This was achieved by bundling the fiber ends, and polishing the ends with 2000 grit sandpaper followed by rubbing with regular print/copy paper.

The fibers were placed in the fiber collars and offset past the collars by 1-2 millimeters before being tightened (but not tight enough to cause damage). Fibers were polished gently in small circular strokes, with frequent visual inspection. Extra care was given to avoid extraneous grit from the sandpaper getting lodged underneath the fiber cladding. It was also found that if the fibers were sanded too quickly, cladding flaring and chipping was possible. As a consequence, the fiber polishing process was done in a slow and careful manner in order to minimize damage to cladding and produce a clean, mirror finish on the fiber ends. Images which show the transition from end-milled cut to polished fibers are shown in Figure 19.

Only one end of the fibers needed to be polished. This was due to the fact that the unpolished ends were going to be fused together and fusing did not benefit from a mirror finish.

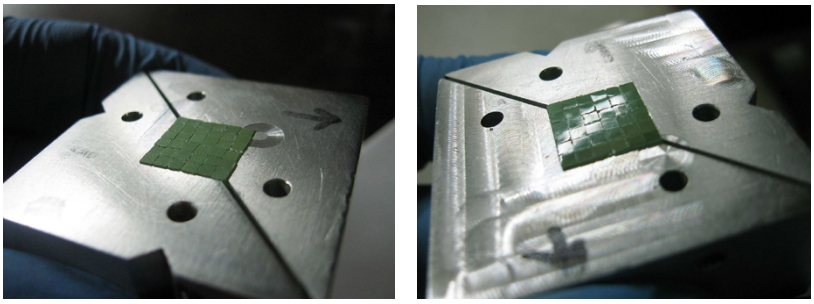

FIGURE 19. Left: A bundle of unpolished scintillating fibers. Right: The mirror finish polish of a bundle of scintillating fibers.

3.7. Fusing

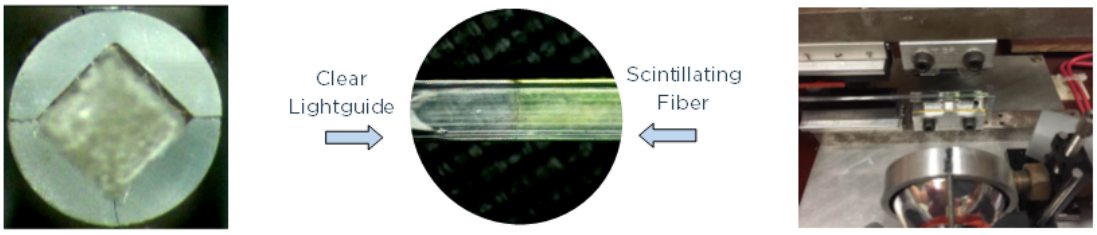

FIGURE 20. Left: A head-on view of a light guide in the square ferrules. Center: An image of a fuse site. Right: A photo of the modified MSU fusing unit.

In order to detect the light pulses collected by the detector, the scintillations created by the scintillating fibers had to be guided to the SiPM photo-sensors. Clear light guides were heated and pushed into the scintillating fibers so their cores were fused together and could transfer the light signal efficiently.

Optical fiber fusing is a standard and important process in any optical fiber system. A fiber fusing unit, originally built at Michigan State University (MSU) for construction of the MINOS experiment, was used to fuse the fibers for the GlueX tagger microscope, see Figure 20. A number of modifications were made to the MSU fusing unit. The most notable modification was the replacement of the quartz ferrules, which MSU had built to hold 1mm diameter circular fibers, with new ones cut to hold square 2mm fibers. It was important that the quartz ferrules be thin and clear to enable light to quickly heat the fiber cores and make them ready to fuse. It was also important that ferrules were precisely machined so when the ferrules were pushed together by a pneumatic piston, the ferrules were aligned so fibers maintained their shape and were not deformed by the pressure and did not leak out of the ferrule when melted by the fuser.

One consequence of the fusing process is a bulge, or widened section at the fuse joint. It's important that the fibers can be packed tightly into a rectangular array so it was necessary to measure and control the size of the fuse site. The fusing process had to be optimized to create strong but small fuse joints. If the fuse process was not done correctly, flared material would be extruded at the corners of the fibers, where the two ferrule-halves come together. The flaring was due to the longitudinal compression force being too high in comparison with the transverse confining pressure applied to keep the two ferrule-halves together. The fiber would not be held in shape by the quartz ferrules and fiber would ooze out and create a lip of flared fiber material. An image of this problem is shown in Figure 21. Some fuses, like the one in Figure 21, which were flared only a slight bit, were salvaged by sanding off just the flared bit of fiber, not touching the fiber fuse at all.

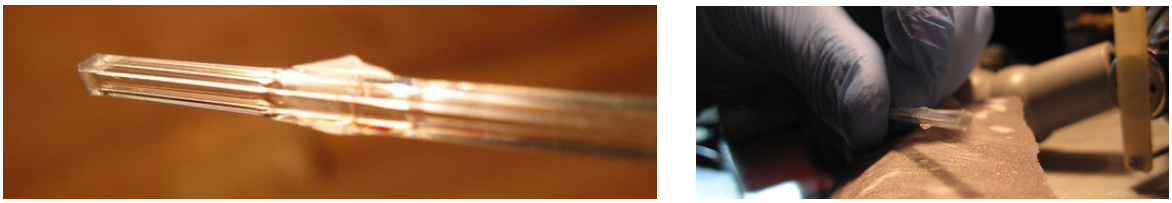

FIGURE 21. Left: The flared lip of an imperfect fuse.
Right: Careful sanding of just the excess fiber to salvage the fiber fuse.

3.8. Bending

Bending the fibers was needed to remove the light guides and photo-sensors from the plane of the incoming electrons. An S-shaped bend was placed right after the fuse site to bend the light guides out of the plane of the incoming electrons, and a large, gentle bend was added further down the light guide so the ends of the light guide fibers would line up properly the photo-sensors. Figure 22 shows an image of the fibers in the bending unit after being bent into the final shape.

The fiber bending process required very meticulous record keeping regarding which fiber was in which position. This allowed us to retain a complete record regarding each fiber's width and production information together with each fiber's final light yield. It was important to keep track of both the position of the scintillating fiber in the matrix of fibers, and also the photo-sensor which is detecting the pulses for each fiber.

A bundling tool was used in the bending process to assist in keeping the fibers aligned and in the right position. The bundling tool is a precision-cut aluminum piece which had a cut-out for an array of 5x6 fibers. Figure 23 shows how the bundling tool had to be filled in order to produce an array of fibers in the order required.

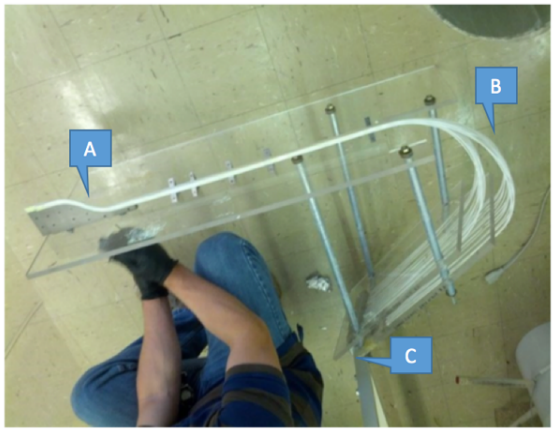

FIGURE 22. An image of the first fiber bundle post-bending. Location A marks the S-bend. Location B marks the larger radius bend. Location C marks where the fibers will be placed over the photo-sensors.

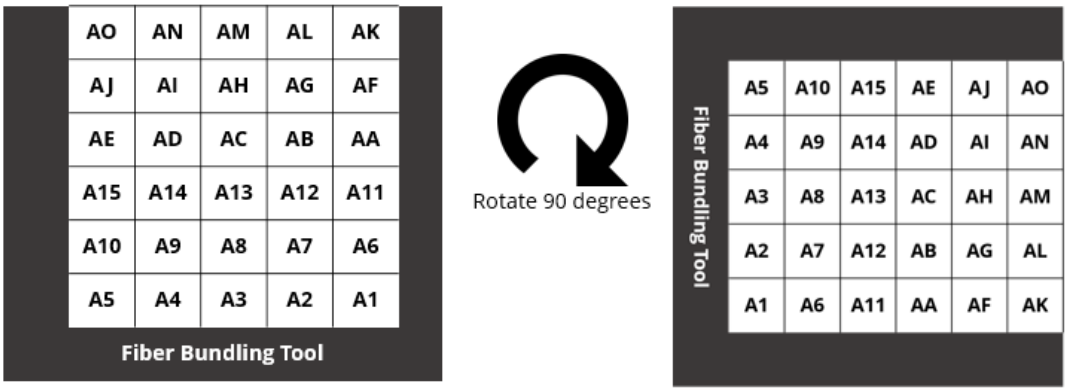

FIGURE 23. Left: The arrangement of fibers in bundling tool, loaded from the bottom up. Right: The desired array of fibers realized after the rotation of the bundling tool.

Once the fibers were properly bundled for bending, they were secured to three plexiglass plates via aluminum fiber collars. The bending plates and collars required for this process are diagramed in Figure 24. The bending unit consisted of 3 plexiglass plates: the bending plate and two chimney plates. The bending plate was the largest. It held the aluminum “popsicle stick” which induced the S-bend on the fiber. The fibers were then split into two groups of 15 and were separated individually by the chimney collars. The chimney collars were attached to two chimney plates. All three plexiglass plates were secured to a large aluminum bar.

After being properly set up, the bending unit was submerged into a large water tank of room temperature water. Originally, the water was just tap water, but as mentioned above, a small water filter was added to the system to minimize hard water and rust effects. Figure 13 shows the layout for the bending tank. Two water heaters and water pumps were used to heat the water in the bending tank up to the appropriate temperature for bending, about 160 degrees Fahrenheit. The same LabVIEW program which controlled the heaters and pumps for straightening was also used for the bending process. This is why the temperature profile for bending is almost identical, see Figure 25.

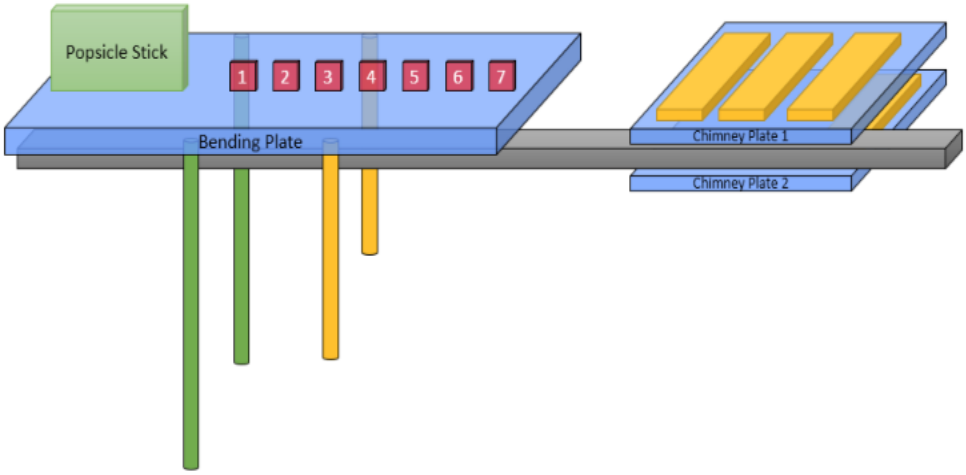

FIGURE 24. A rough diagram of the bending unit and all its parts (the fibers are not shown). On the bending plate is the "popsicle stick" which induces the S-bend into the fiber as well as 7 fiber collars which maintain the fiber's 6x5 arrangement. There are 3 chimney collars on each of the two chimney plates which separate the 6x5 arrangement into two sets of 15 individually spaced fibers (15 fibers/plate).

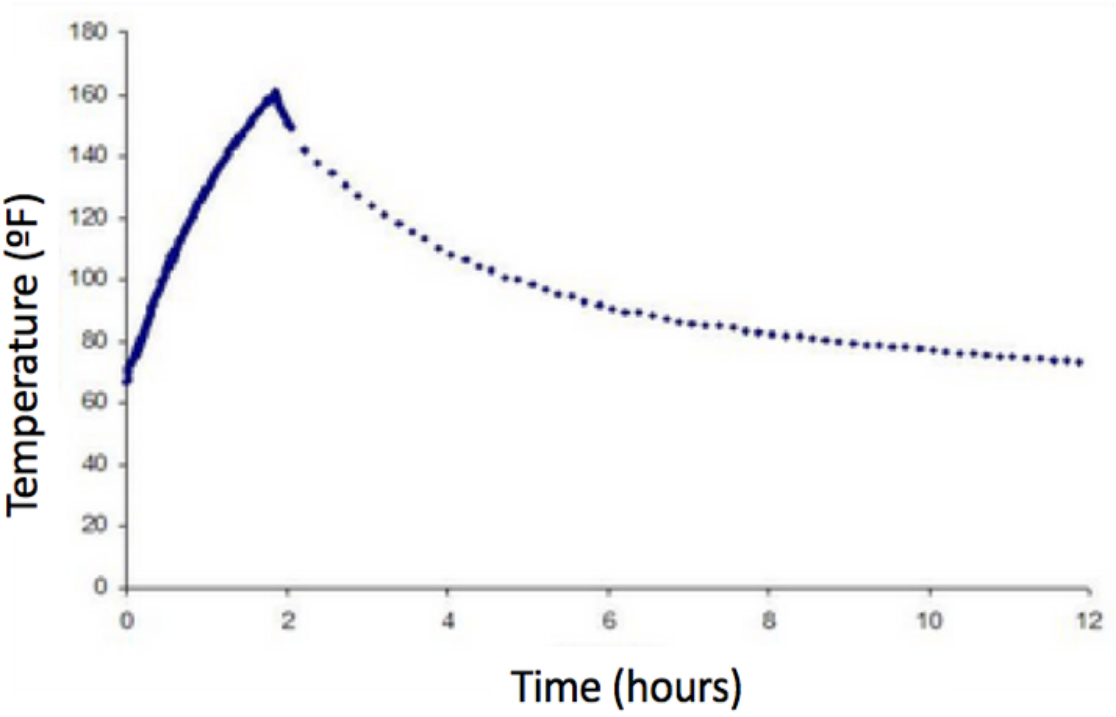

FIGURE 25. Temperature time series throughout the bending procedure of bundle 1.

Once the bending unit was at the right temperature for bending and the fibers were malleable, the bending unit had to be switched from the straight to the bent configuration. The unit was removed from the water and the chimney plates were removed from the fixed bar and pivoted to its bent position above the popsicle stick plate. The S-bend was also carefully created by squeezing together two complementary S-shaped aluminum pieces surrounding the fibers. A rendered diagram of the process needed to create the large bend is shown in Figure 26. The entire process took about 5 minutes, and then the fibers were placed back into the water, to cool down to room temperature again and allow the fibers to anneal into their new shape.

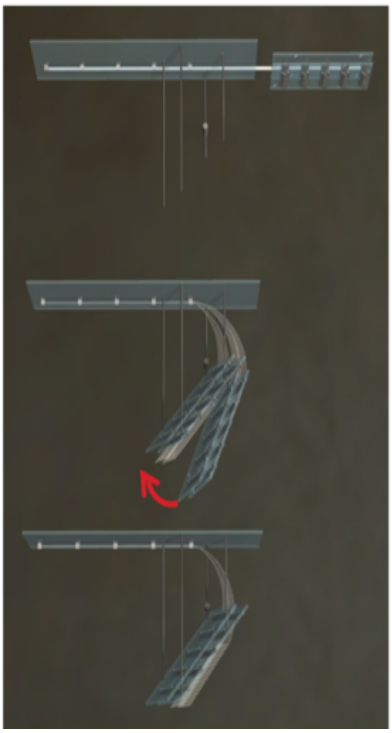

FIGURE 26. A rendering of the chimney plates being secured to the bending plate.

3.9. Painting and Gluing

The original prototype construction procedure for the tagger microscope included painting and gluing of the fibers after the bending procedure. The fibers were to be covered with a thin layer of white acrylic paint to minimize cross-talk between fibers and then glued together in rectangular blocks of 5x6 fibers to make transport and handling easier.

However, these two steps had to be eliminated from the fiber production procedures due to a number of problems that resulted from their use. With regards to painting, it was difficult to apply a thin, even coat to the fibers. A 50/50 mixture of white titanium dioxide paint and water was

spray-painted onto the fibers in hopes of creating a thin yet opaque and even coating. The results were paint layers which were too thick and varied too greatly from fiber to fiber. The paint was also easily blemished during handling and testing, which was an issue (Figure 27).

FIGURE 27. A photo of a painted fiber with blemishes from handling and measurement.

The fibers were originally planned to be glued to the popsicle stick to provide structural support for the fibers near the fuse joint and the S-bend using the Saint Gobain Inc. BC-600 optical cement. This optical cement is generally used to form optical joints between sections of plastic scintillator. However, adding the glue between the fibers eliminated the air boundary-layer around the fibers which greatly reduced their light capture fraction, resulting in a significant decrease in the number of photons per pulse observed at the sensor. As a result, both processes were removed from the production procedures.

4. Testing and Installation

Once the fibers were bent, they had to be mounted into the laser pulse testing unit at UConn for quality assurance testing. Images of the UConn testing unit are displayed in Figure 28. The testing unit included two readout boards, each with 15 photo-sensors, which allowed 30 fibers could be tested at a time.

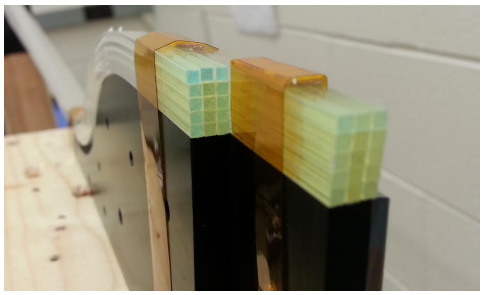

FIGURE 28. A bundle of optical fibers mounted onto a popsicle stick for testing at UConn.

A fast-pulsed laser diode was used as a source to measure the fibers' relative transmission yield at the photo-sensors. Fibers were secured onto a coated aluminum "popsicle stick" which was cut to match the S-bend of the fibers. One difference between the final testing "popsicle sticks" and the

bending “popsicle stick” is that the testing popsicle sticks grouped the 30 fibers into two sets of 15 as per the photo-sensor boards. The fibers were secured to these popsicle sticks using thin straps of non-adhesive kapton strips, see Figure 29. Small pieces of thin wood (sections of wooden coffee stirrers) were placed on top of the kapton strips to keep the center column from becoming offset. Thin pieces of index card paper were also put between the columns and rows of the fibers near the S-bend to create a small air gap and minimize cross-talk between the fibers.

The testing unit at UConn measured the relative transmission yields for each fiber. The photon yield for all 622 fibers produced are shown in Figure 29. As shown, the majority of the fibers produced had a photon yield of 500 counts or less.

Benefits of the production process changes are observed when comparing the fibers produced first to the fibers produced after installation of the water filter, the removal of painting, etc. The 209 fibers which were painted had an average photon yield of 252 counts. Compared to the non-painted fibers, which averaged 606 counts, the devastating effects of the painting process become clear and quantifiable. The tagger microscope was installed in Hall D of Jefferson National Laboratory in August 2014 by Dr. Richard Jones, James McIntyre, Alex Barnes, and Brendan Pratt. Figure 30 is a photo of the detector fully constructed at JLab and ready to be installed. Once installed, further testing and calibration of the detector was and is currently being conducted by Alex Barnes.

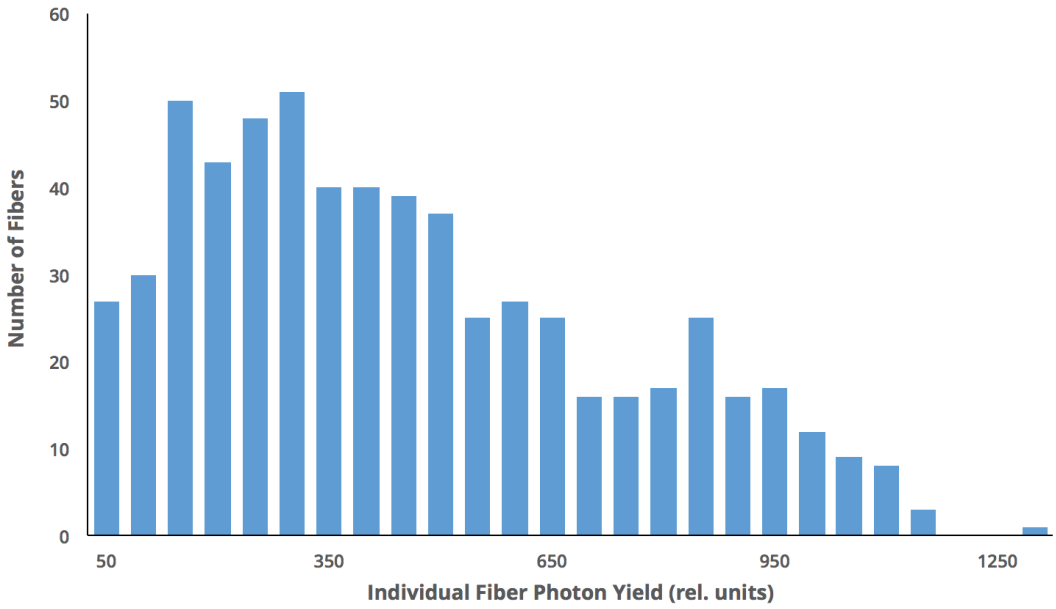

FIGURE 29. A histogram of the photon yields for the 510 fibers produced. The average photon yield was 490 counts and the median was 450. Future production efforts aim to replace the fibers performing in the lower 60th percentile, which equates to fibers performing below 500.

FIGURE 30. An image of the complete tagger microscope about to be installed in Hall D.

5. Conclusion

It was discovered during testing that the collected light yield in the tagger microscope varied by as much as a factor of 5 from one fiber to the next, see Figure 29. Despite the adjustments made to the fiber production process (removing the painting and gluing steps, changing cleaning procedure and adding water filters) to increase efficiency, only about half of the fibers were meeting minimum specifications for light yield. It was determined that this underperformance issue was due to the lack of second cladding layer on the fibers and due to the hot water treatment the fibers endured.

Once the manufacturer confirmed the fibers were not multi-cladded, the correct shipment of multi-cladded fibers was sent to UConn in September 2014. The second cladding layer of the new fiber shipment was confirmed at UConn, see Figure 28. The detector as currently installed at JLab is performing at a level sufficient for commissioning the tagger, but UConn is preparing a new set of replacement fibers to be installed in time for the first physics data-taking run in 2016.

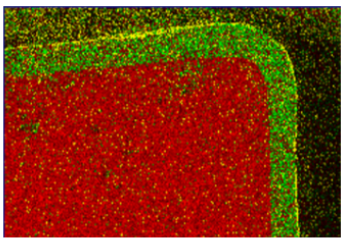

FIGURE 31. An x-ray diffraction scan of the cross section of a multi-cladded fiber. In this image the fluorine in the fluor-acrylic 2nd cladding layer is shown in yellow. Although thin, the existence of the second cladding layer is confirmed.

These updated construction procedures eliminate the hot water treatment of the fibers as it was found this introduced the largest amount of fiber stress. The new fibers will no longer be straightened or bent in hot water. Rather, the fibers will not be straightened and will only have the S-bend. The fibers will be heated to temperature using a hot air system rather than a hot water system to reduce rust, hard water stains, and internal stress. The production of a set of new, multi-cladded fibers is ongoing at UConn as of December 2015. These re-production efforts should result in the replacement of approximately ten 30-fiber bundles (around 60%) of low signal transmission fibers with fibers whose photon yields are comparable or better to the fibers produced at the end of this production run.

6. Acknowledgements

First and foremost, I'd like to thank Dr. Richard Jones for accepting me into his research group when I was a young, inexperienced freshman and for providing excellent opportunities to learn about and participate in experimental physics throughout my entire college career. Within his research group, I'd like to thank graduate students James McIntyre, Alex Barnes, and Fridah Mokaya, all of whom were happy and eager to teach me and help when needed. I'd also like to thank Ann Marie Carroll, my supervisor and friend, with whom I spent many hours with in the lab while working on fibers. Thank you for teaching me and my fellow undergraduate researchers: Ben Willis, Jonathan Kulakofsky, John Bartolotta, Kenny Brand, Aaron Khan, and Andrew Sampino. And of course, I send my thanks to my cousin, Brendan Pratt, for nurturing my interest in science over the years and for introducing me to Dr. Jones' research group in 2012.

I'd also like to thank the National Science Foundation for funding the GlueX project. My work could not have been completed if not for the PHY-120785 grant which we received. I'd also like to thank the UConn Honors program and the UConn Physics Department for providing excellent services and sense of community which allowed me to excel at UConn and find my niche at such a large public university.

And finally, I want to thank my parents, Lou and Theresa Hotte and my sister and brother-in-law Jessica and Yli Schwartzman. Thank you for always asking about the lasers, diamonds, and fibers that Brendan and I worked on and for always being there for me. I could never have been as successful at UConn without your constant love and support.

7. References

AIP. (1997, March). *A Look Inside the Atom*. Retrieved from https://www.aip.org/history/electron/jjhome.htm

CODATA. (2015, July 27). *Fundamental Physical Constants - Speed of Light in Vacuum*. Retrieved from NIST Reference on Constants, Units and Uncertainty: http://physics.nist.gov/cgi-bin/cuu/Value?c

Halliday, D., Resnick, R., & Walker, J. (2010). *Fundamentals of Physics* (9th ed.). Wiley.

Jefferson Lab. (2013, September 20). *12 GeV Upgrade*. Retrieved from Jefferson Lab - Office of Science DOE: https://www.jlab.org/div_dept/physics_division/GeV/index.html

Perkins, D. H. (1982). *Introduction to High Energy Physics* (2nd ed.). Addison-Wesley.

Purdue University. (n.d.). *Ernest Rutherford*. Retrieved from http://chemed.chem.purdue.edu/genchem/history/proton.html

Riordan, M. (1992, April). The Discovery of Quarks. *SLAC-PUB-5724*. Retrieved from http://www-spires.slac.stanford.edu/cgi-wrap/getdoc/slac-pub-5724.pdf

Senderovich, I. (2012). A Polarized High-Energy Photon Beam for Production of Exotic Mesons. *UConn Doctor of Philosophy Dissertation*.

Underwood, M. (2010). Design of Electronics for High-Energy Photon Tagger for the GlueX Experiment. *UConn Honors Scholar Thesis*. Retrieved from http://digitcalcommons.uconn.edu/srhonors_theses/163

University of California - Santa Barbara. (n.d.). *Who discovered electrons, protons and neutrons?* Retrieved from UCSB ScienceLine: http://scienceline.ucsb.edu/getkey.php?key=408